Review article

Eugenio Calandrini[a], Andrea Cerea[a], Francesco De Angelis, Remo Proietti Zaccaria and Andrea Toma*

Magnetic hot-spot generation at optical frequencies: from plasmonic metamolecules to all-dielectric nanoclusters

https://doi.org/10.1515/nanoph-2018-0138
Received September 7, 2018; revised October 26, 2018; accepted November 1, 2018

Abstract: The weakness of magnetic effects at optical frequencies is directly related to the lack of symmetry between electric and magnetic charges. Natural materials cease to exhibit appreciable magnetic phenomena at rather low frequencies and become unemployable for practical applications in optics. For this reason, historically important efforts were spent in the development of artificial materials. The first evidence in this direction was provided by split-ring resonators in the microwave range. However, the efficient scaling of these devices towards the optical frequencies has been prevented by the strong ohmic losses suffered by circulating currents. With all of these considerations, artificial optical magnetism has become an active topic of research, and particular attention has been devoted to tailor plasmonic metamolecules generating magnetic hot spots. Several routes have been proposed in these directions, leading, for example, to plasmon hybridization in 3D complex structures or Fano-like magnetic resonances. Concurrently, with the aim of electromagnetic manipulation at the nanoscale and in order to overcome the critical issue of heat dissipation, alternative strategies have been introduced and investigated. All-dielectric nanoparticles made of high-index semiconducting materials have been proposed, as they can support both magnetic and electric Mie resonances. Aside from their important role in fundamental physics, magnetic resonances also provide a new degree of freedom for nanostructured systems, which can trigger unconventional nanophotonic processes, such as nonlinear effects or electromagnetic field localization for enhanced spectroscopy and optical trapping.

Keywords: magnetic hot-spots; artificial optical magnetism; Fano resonance; Mie resonances.

1 Introduction

In the optical range, light-matter interactions are mostly mediated by the electrical polarizability of atoms and molecules induced by the electric component of an incident electromagnetic (EM) field. This characteristic has been exploited in the past years to engineer the spectral response of materials and boost their EM behavior at the nanoscale, by carefully adjusting their inherent features (refractive index, free-carrier density, etc. [1–6]) and their structural parameters (size, shape, etc. [7–9]). In this respect, much attention has been devoted to the study and optimization of localized surface plasmon resonances (LSPRs) of metallic nanostructures [10, 11] and Mie resonances of their dielectric counterparts [12]. In both cases, interaction with an incident EM field at the right frequency causes accumulation of charges of opposite signs in different regions of the nanoparticle, thus giving rise to an effective electric polarization. The key property of these resonances is the ability to concentrate light in sub-wavelength regions, called hot-spots [13], with electric field intensities that are enhanced up to several orders of magnitude. This effect has been largely exploited for biosensing [14], light harvesting

[a]**Eugenio Calandrini and Andrea Cerea:** These authors contributed equally to this work.
***Corresponding author: Andrea Toma,** Istituto Italiano di Tecnologia, Via Morego 30, 16163 Genova, Italy,
e-mail: andrea.toma@iit.it. https://orcid.org/0000-0003-2877-9805
Eugenio Calandrini and Andrea Cerea: Istituto Italiano di Tecnologia, Via Morego 30, 16163 Genova, Italy; and Dipartimento di Informatica, Bioingegneria, Robotica e Ingegneria dei Sistemi (DIBRIS), Università degli Studi di Genova, Via All'Opera Pia 13, 16145 Genova, Italy
Francesco De Angelis: Istituto Italiano di Tecnologia, Via Morego 30, 16163 Genova, Italy
Remo Proietti Zaccaria: Istituto Italiano di Tecnologia, Via Morego 30, 16163 Genova, Italy; and Cixi Institute of Biomedical Engineering, Ningbo Institute of Materials Technology and Engineering, Chinese Academy of Sciences, Ningbo 315201, China

applications [15], photocatalysis [16] and non-linear light generation [17], just to mention a few applications.

On the contrary, interaction with the magnetic component of light in natural materials is rather weak and is greatly limited by the small value of the magnetic permeability μ at optical frequencies. This is an intrinsic constraint due to the asymmetry between electric and magnetic effects. Although reaching optical magnetic phenomena may seem unrealistic, through the employment of properly designed materials, it is possible to suitably engineer displacement and conduction currents, achieving enhanced magnetic dipole moments even though the constituting elements are not endowed with microscopic magnetization [18, 19]. Within this framework, the non-local response [20], i.e. spatial dispersion, of artificially designed materials can act as a source of optical magnetism in response to EM field irradiation. Interestingly, recent advances in nanofabrication techniques have paved the way towards the realization of artificial optical materials [21] exhibiting a magnetic behavior even in the visible spectral range, thus enabling the experimental realization of previously inconceivable phenomena, such as negative [22, 23] and near-zero refractive index [24, 25], hyperbolic dispersion [26, 27] and "gap-mediated" meta-molecules, [28, 29] with breakthrough applications in many fields of optics [30–35].

The possibility of creating materials simultaneously featuring negative values of electrical and magnetic permeabilities was envisioned by Veselago [36] in the 1960s, stimulating the interest of the scientific community in this field of science. Following this idea, the first architecture endowed with these characteristics was proposed in 1999 by Pendry [37], who conceived and introduced the split-ring resonator (SRR) layout, i.e. a microscopic metallic ring-like structure resembling a coil (see Figure 1A). When

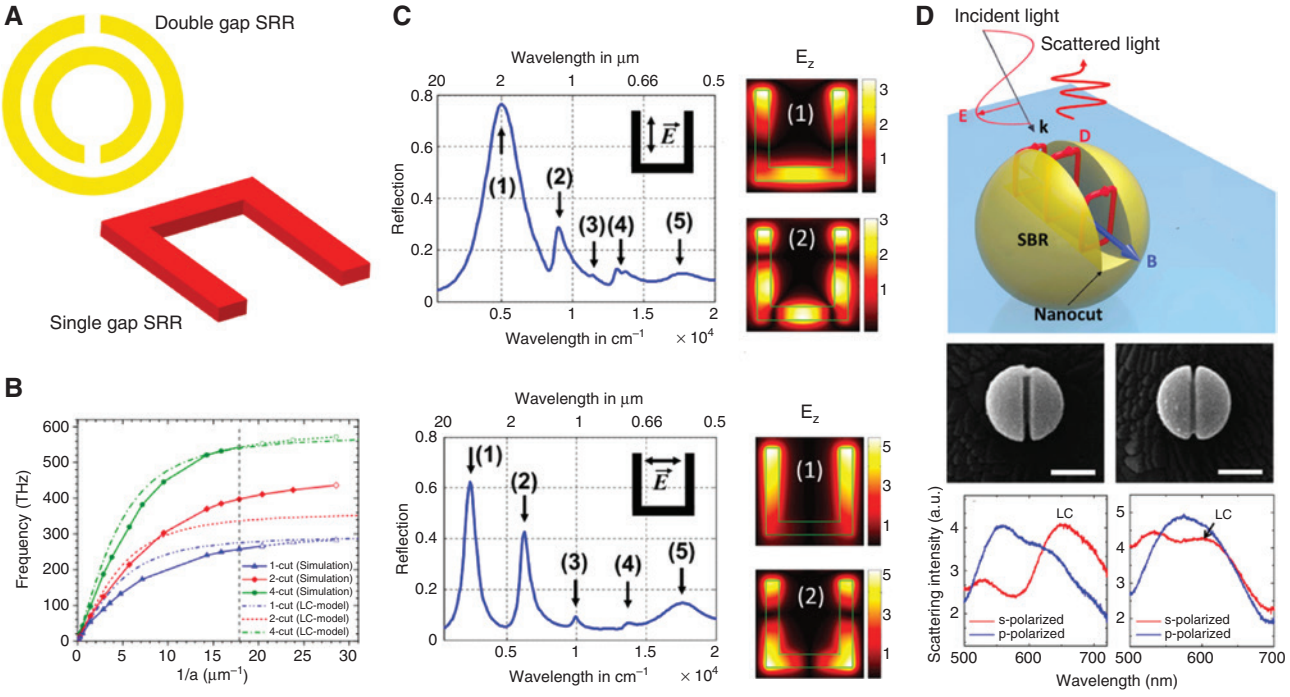

Figure 1: Planar and 3D split ring resonator (SRR).
(A) Top, the SRR originally proposed by Pendry [37]. Bottom, low footprint version of SRR, suitable for scaling the device to target the optical range [38]. (B) The spectral shift of the magnetic resonance mode with respect to the SRR size. Despite the increase in the number of gaps in order to reduce the net capacitance of the system, the linear scaling law holds only in the low energy limit. Reprinted with permission from Zhou J, Koschny T, Kafesaki M, Economou EN, Pendry JB, Soukoulis CM, Phys Rev Lett, 95, 223902, 2005. Copyright 2005 by the American Physical Society (Ref. [39]). (C) Top, spectral distribution for the first five modes excited under the $E_{\perp}$ polarization and near-field maps of the absolute value of the local E field normal component for the first two modes. Bottom, spectral distribution for the first five modes excited under the $E_{//}$ polarization and near-field maps of the absolute value of the local E field normal component for the first two modes. Adapted with permission from Ref. [38], 2006 Optical Society of America. (D) Top panel, schematic of the Split Ball Resonator, the 3D analogue of the planar SRR. The cut in a gold nanoparticle was performed through Focused Helium Beam milling, resulting in a low defect architecture (middle panel). Bottom panel, scattering spectra of the two particles in the middle panel for incident s- (red curves) and p-polarized (blue curves) light. The accuracy of fabrication enables the device operation at optical frequencies. Panel (D) has been reprinted by permission from Springer Nature, Nat Commun 2014;5:3104 Split-ball resonator as a three-dimensional analogue of planar split-rings. Kuznetsov AI, Miroshnichenko AE, Fu YH, et al. (Ref. [40]) Copyright (2014) Springer Nature Limited.

incident light is coupled to this system, a resonant circulating current is excited and gives rise to an oscillating magnetic field in the center of the ring, thus mimicking an oscillating magnetic dipole. To date, several alternative designs have been proposed in order to optimize the magnetic response of SRR and its unusual properties, such as negative refraction [22], cloaking [41], or superlensing [42]. The SRR concept works well in the infrared regime, but almost fails in the visible spectral range as a result of increased radiation losses and fabrication issues. In order to overcome these difficulties, a proposed solution relied on the introduction of metallic nanostructure assemblies [43–47]. These multiparticle arrangements are usually called metamolecules or plasmonic oligomers, and their EM properties depend on the mutual interaction between the constituting sub-units. When the nanoparticles are closely packed together and arranged in circular loops, plasmons start to synergistically interact, thus forming collective modes, which can be magnetic in nature. Unlike the SRR case, magnetic modes are not induced by a conduction current but instead by a resonant displacement contribution. This property helps achieve sharp magnetic resonances [48] at visible frequencies with lower intrinsic losses, higher sensitivity to the local dielectric environment and enhanced magnetic fields at the center of the nanostructure assembly [49]. The quest for magnetic resonances at visible frequencies has drastically reduced the required dimension of nanostructured sub-elements within the metamaterial unit cell, especially in the case of near-field coupled structures (i.e. oligomers), whose fabrication tolerances must be tailored down to the sub-nm resolution. In this respect, in order to reduce the intrinsic broadening of their spectral features due to fabrication challenges (i.e. to achieve improved quality factor), alternative designs and high resolution techniques have been developed, such as monolithic resonators [50], He beam patterning [40] and atomic force microscope (AFM) nanomanipulation [51].

Despite the advantages offered by metallic nanoparticle oligomers, the inherent losses at visible wavelengths associated to noble metal plasmonic materials, such as gold and silver, severely affect their straightforward translation into practical applications. On the contrary, high-refractive index dielectric materials offer an alternative route to achieve a strong magnetic response in this frequency window [52, 53], thereby overcoming critical issues, such as heat dissipation and radiation losses [54–56]. In contrast to “conventional” plasmonic materials/structures, in purely dielectric systems only displacement currents contribute to the magnetic moment of the artificial material and even simple spherical dielectric nanoparticles can support both electric and magnetic Mie resonances without the need of complex architectures. In this case, the lowest order resonance is a magnetic dipole, generated by circulating displacement currents, which enhance the magnetic field at the nanoparticle center [57]. Moreover, near-field coupling between dielectric nanoparticles helps generate strong magnetic hot-spots confined in the inter-particle regions [57], similar to the electric hot-spots associated to their metallic counterparts. The interference of electric and magnetic modes supported by these assemblies can give rise to sharp Fano resonances with a magnetic nature [58–60], and offer new opportunities, such as wavefront manipulation of light [56, 61–63], ultrafast all-optical switching [64, 65] and optical magnetic mirrors [66].

So far, different approaches have been followed to achieve advanced control of the magnetic component of light at the nanoscale level. In this review, we will try to give an exhaustive overview of the main achievements that lie behind magnetic hot-spot generation. In particular, we will focus on magnetic resonances sustained by artificial materials in the infrared and visible spectral range, with specific emphasis on plasmonic metamolecules and all-dielectric nanoclusters. Concurrently, we briefly present some of the many inspiring results which are paving the way towards important applications in the fields of surface enhanced spectroscopies [67], non-linear light generation [68–71] and optical trapping [72, 73].

2 Split-ring resonator

The first evidence of artificial magnetism at optical frequencies was provided in 1999 by Pendry et al. with the aim of finding the magnetic analogue of a good electrical conductor [37]. The architecture proposed was a SRR, i.e. an artificially produced structure consisting of a couple of metallic concentric loops with splits at the opposite ends (see Figure 1A, top). An alternative simplified version of the double-ring resonator, consisting of a single SRR with one cut, was introduced and investigated in later works [38, 39, 74] (see Figure 1A, bottom). In particular, the spectral response of U-shaped SRRs for impinging light at normal incidence with respect to the structure plane has been studied both numerically [38] and experimentally [74]. The presence of a gap enables the identification of two different illuminating conditions, where the electric field is respectively perpendicular ($E_{\perp}$) or parallel ($E_{//}$) to the ring disconnection. The modes sustained by SRRs are displayed in Figure 1C, which shows that, while an electric dipolar

configuration is excited for impinging orthogonal polarization - $E_{\perp}$ (Figure 1C - top panel - resonance (1)), a strong magnetic contribution (the so-called "LC-resonance" of the SRR) is manifested under $E_{//}$ irradiation (Figure 1C - bottom panel - resonance (1)). In this case, the structures can support circulating currents, thus enriching their EM response with a clear magnetic character. Starting from these pioneering works, many other results demonstrating a magnetic resonance of metallic structures have been reported, especially in the infrared and microwave regions [75–78]. The SRR EM response can be intuitively explained through a lumped element LC-analogue [79]. Given that the gap acts as a capacitor C and an inductance L can be assigned to the metal ring, the resonance frequency of the system can be approximated by $\omega = 1/\sqrt{LC}$, which exclusively depends on the SRR size/geometrical parameters. Under this assumption, a simple approach to shift the SRR resonance towards visible frequencies consists in the *ad hoc* fabrication of smaller structures. Concurrently, a complementary strategy to increase the operation frequency of an SRR involves the number of gaps: based on the lumped element model introduced above, an increasing number of gaps results in a series of capacitors, and a consequent reduction of the system net/total capacitance. Following this idea, Zhou et al. [39] numerically investigated the spectral response of multi-cut SRRs, achieving magnetic resonances up to visible frequencies. These concepts are well described in Figure 1B, where the SRR magnetic resonance frequency, f_m, *is* plotted as a function of the linear ring size, a, and the number of splits. Up to the lower THz range, a linear dependence $f_m \propto 1/a$ can be immediately recognized, whereas a clear saturation appears for higher frequencies. The electron self-inductance as well as the additional losses intrinsically connected to nanosized plasmonic materials severely jeopardize the immediate extension, through a direct geometrical rescaling, of the resonant magnetic response of metallic nanostructures into the visible spectral region. Recently, new perspectives for light manipulation at the nanoscale have been promoted by the significant advancements in modern nanofabrication techniques [80], which help enrich the fabricated structures with high-quality details and/or complex architectures [81–85]. A crystal-clear example is offered by the extremely precise nano-cut introduced on top of a spherical plasmonic nanoparticle [40], the so-called split ball resonator (SBR), whose spectral behavior has been observed to be very similar to that of a conventional SRR. A schematic illustration of the present architecture, together with a representative helium ion microscope image, is depicted in Figure 1D, where a clear analogy to a 3D upright SRR can be immediately noticed. On the one hand, for an impinging electric field that is polarized parallel to the nanogap plane (p-polarized configuration), the optical response of the proposed structure exhibits a resonance peak associated to an electric dipole (blue curves in Figure 1D). On the other hand, for an incoming polarization perpendicular to the cut (s-polarized configuration), two resonant features appear in the scattering spectrum: a weak resonant peak close to the position of the electric resonance and a more pronounced one at longer wavelengths corresponding to the LC (i.e. magnetic) response (red curves in Figure 1D). This result fully recovers the optical behavior of the SRR and allows the extension of the device frequency operation up to the visible region of the EM spectrum [40]. Moreover, the present architecture, with its intrinsic 3D nature, offers a more efficient coupling to the impinging radiation for both electric and magnetic contributions. Indeed, the SBR can be excited for all incident directions lying in the plane parallel to the nano-cut. The performance of this kind of structure in terms of field enhancement at the magnetic resonance frequency ranges between 20 and 45, a value which is fully consistent to analogous results retrieved in the near-infrared spectral range [76, 86]. In addition, a wide tunability throughout the whole optical window can be obtained, depending only on the nanostructure geometrical parameters, such as the nano-cut width and depth.

Despite the promising characteristics and the relatively simple design offered by SRRs, alternative [87, 88] and/or more complex configurations [18] have been concurrently conceived and investigated, in order to push even further the advanced control of the magnetic component of light at the nanoscale level.

3 Metamolecules and plasmonic oligomers

In the same way in which the SRR resembles an elemental coil, other architectures can be directly inspired by nature analogues, thus encouraging the quest for new artificial magnetic phenomena at visible and/or infrared frequencies. For example, aromatic molecules formed by multiple rings of six carbon atoms can trigger current loops, which are supported by the electrons of the delocalized π orbitals, interacting with a magnetic field and inducing a magnetic response. In this view, with the aim of replicating these natural systems, plasmonic hexamers [43, 44] and/or heptamers [45–47] can be introduced as benzene-analogue building blocks for the construction of cyclic aromatic structures of increasing complexity (see Figure 2). These multiparticle architectures are usually called

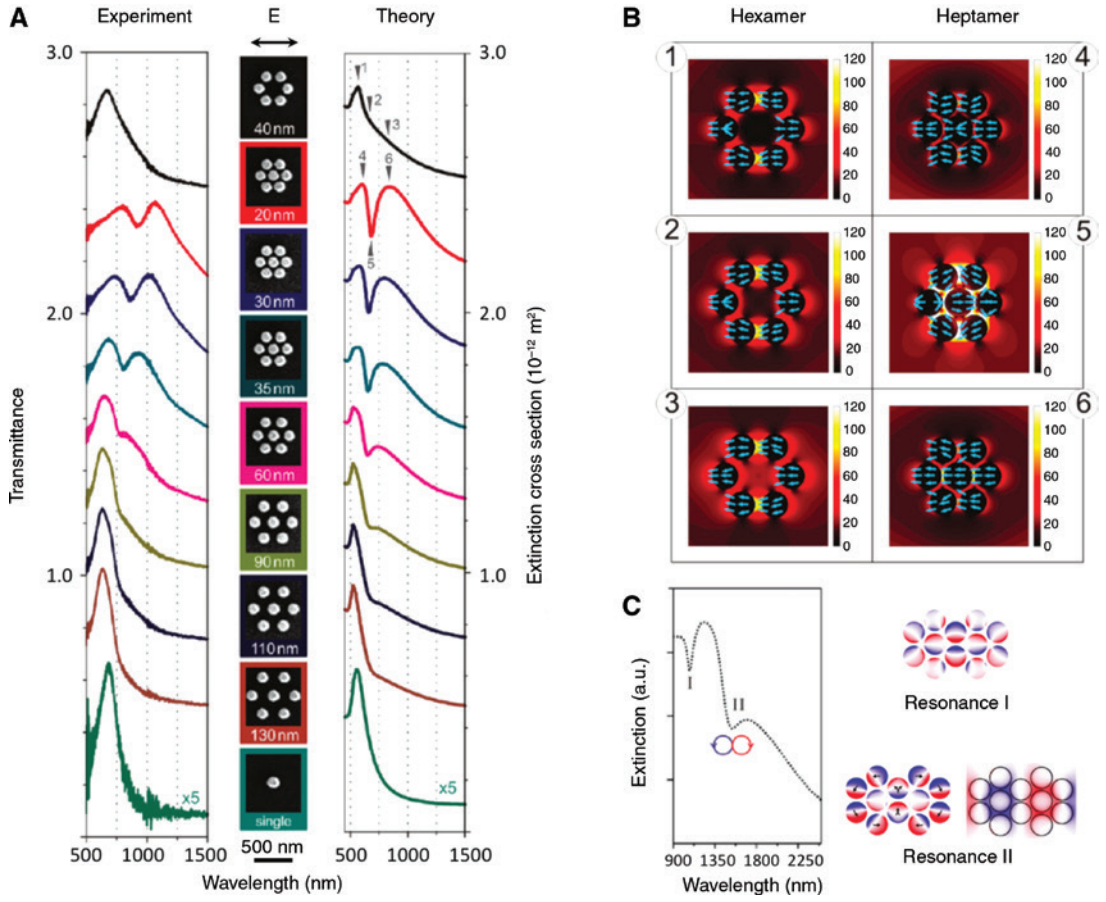

Figure 2: Plasmonic oligomers and displacement currents.
(A) Measured and simulated transmittance spectra of an array of heptamers at normal incidence, upon inter-particle gap reduction (brown to red curves). The onset of the Fano resonance is clearly visible for gaps below 90 nm. Both the monomer and the hexamer structures feature a single peak in their corresponding transmittance spectra (aquamarine and black curves, respectively). (B) Near field distribution at the selected wavelengths reported in (A) for both the hexamer and the heptamer. The presence or absence of the Fano resonance is due to the central nanoparticle. The superradiant and subradiant modes that destructively interfere, hence giving rise to the Fano resonance, are characterized by the plasmon on the central nanoparticle oscillating in-phase or in counter phase with respect to the six satellite nanoparticles, respectively. Adapted with permission from Hentschel M, Saliba M, Vogelgesang R, Giessen H, Alivisatos AP, Liu N. Transition from isolated to collective modes in plasmonic oligomers. Nano Lett 2010;10:2721–6 (Ref. [47]). Copyright 2010 American Chemical Society. (C) Simulated extinction spectrum of a naphthalene-like oligomer (left) and charge densities and magnetic field plots at resonances I and II (right). Adapted with permission from Liu N, Mukherjee S, Bao K, et al. Magnetic plasmon formation and propagation in artificial aromatic molecules. Nano Lett 2012;12:364–9 (Ref. [89]). Copyright 2012 American Chemical Society.

metamolecules or plasmonic oligomers, and their optical properties are defined by the relative position of each sub-unit, in the same way in which the relative position of atoms defines the properties of a molecule. This analogy is surprisingly convenient in describing the near-field interaction of plasmonic nanoparticles. Once they are brought into close proximity, plasmons start to interact with each other and form hybridized collective modes, similar to molecular orbitals. This behavior is clearly visible in the case of a heptamer, whose extinction spectrum exhibits the onset of an extra transparency dip for interparticle separations below 60 nm (Figure 2A, brown to red configurations). The obtained optical response can be ascribed to the interference between a bright "super-radiant" and a dark "sub-radiant" plasmon, i.e. between collective resonances that efficiently couple or not to the incoming light. The archetypical features of these modes can be summarized as follows: a sub-radiant (dark) mode originates from an EM configuration, in which the super-position of the electric dipole momenta supported by the system sub-units is vanishing, as opposed to the radiant (bright) case, where the system possesses a net dipole contribution. As a consequence, the coupling efficiency with the impinging radiation is completely different: a sub-radiant mode poorly responds to external EM radia-tion due to its negligible electric dipole moment. The

interference between bright and dark modes corresponds to a typical Fano resonance condition [90, 91]. Indeed, Fano resonances are normally caused by strong interaction between a narrow/discrete and a broad/continuum of states, which are spectrally overlapped, and lead to the formation of a pronounced dip (extra-transparency) in the extinction response of the system. This concept is even more evident if we observe the near-field characteristics of "aromatic metamolecules" (as depicted in Figure 2B). Indeed, we can immediately recognize that the dipolar plasmon of the central nanoparticle hybridizes with the surrounding hexamer, giving rise to in-phase (Figure 2B, panels 4 and 6) or out-of-phase (Figure 2B, panel 5) oscillating currents, which are respectively associated to radiant and sub-radiant modes of the overall assembly. Obviously the latter configuration is forbidden in the bare hexamer, where only a concordant motion of the free electron charges is allowed (Figure 2B, panels 1–3).

Even more interesting phenomena arise from the mutual interaction between adjacent benzene-like building blocks, resembling the characteristics found in aromatic hydrocarbon molecules [89]. For instance, the plasmonic analogue of naphthalene, i.e. a bicycling ring with two shared atoms, can support two Fano resonances (denoted as resonances I and II in Figure 2C) that are well separated in frequency. While resonance I corresponds to a charge distribution in which the central particles are in an antiphase configuration with respect to the surrounding ones, resonance II is characterized by ring displacement currents circulating in opposite directions, leading to the excitation of two antiparallel magnetic moments. For increasing number n of heptamer sub-units, multiple sub-radiant modes appear in the simulated absorption spectrum of the entire assembly, and the ring magnetic mode is sustained only by the metamolecules with even values of n. Finally, in the case of a 12-heptamer chain excited at normal incidence with linearly polarized light, the optical response is characterized by a magnetic resonance, in which every sub-unit supports a current loop. The induced magnetic moments are aligned in a fully antiparallel symmetry, resulting in an "anti-ferromagnetic" plasmonic system. The efficient near-field coupling between adjacent nanoparticles helps overcome the intrinsic limitations of noble metals at visible frequencies by converting the conduction currents, usually employed in SRRs, into their displacement counterparts, still supporting an efficient magnetic coil-like resonance [18, 92]. Moreover, the sub-radiant nature of these modes guarantees high propagation lengths, making the system eligible for integrated optical devices or waveguide applications.

With the aim of properly explaining the near-field coupling between radiant and sub-radiant modes, it is worthy to consider a simpler architecture consisting of four closely packed nanoparticles arranged in a ring configuration, as depicted in Figure 3, a particular arrangement extensively reported in the literature [51, 92, 94, 95]. The optical response of this system is entirely determined by the overall geometry, where smaller displacements (in the order of 1 nm) of a single nanoparticle unit result in drastic changes of the spectral read-out. The recent results by Alù and coworkers, who have exhaustively studied a plasmonic quadrumer from both the experimental and the numerical standpoints [51, 93], offer a clear example in this direction. Even though this peculiar architecture has already been fabricated by using top-down and bottom-up approaches, the extreme control of the individual nanoparticles, offered by atomic force microscope positioning (see Figure 3A), has allowed a clear-cut investigation of different geometrical configurations [51]. When the nanoparticles are placed far apart, the scattering spectrum is characterized by a single, broad resonance arising from the dipolar contribution of the individual nanoparticles, as shown in the scattering spectra of Figure 3B (left). Reduction of the interparticle gaps results in a red-shift of the electric dipole resonance. This behavior can be associated with an increase of the capacitance induced by the nanostructures mutual coupling, as predicted by the lumped element LC-analogue. For sub-10 nm interparticle separations, the collective plasmon response exhibits a pronounced Fano dip in the scattering spectrum (see Figure 3B, right), originating from the hybridization between a radiant (broad) electric dipole and a sub-radiant (narrow) magnetic mode. Namely, the structure proposed in Figures 3A–B exhibits strong electric and magnetic responses, which are spectrally overlapped in the visible frequency range. In an ideally symmetrical configuration, these modes are orthogonal and additively contribute to the total scattering cross-section without interference and the entire molecule simply acts as a single isolated dimer (see Figure 3C, left panels). Therefore, the most efficient way to excite magnetic-based Fano resonances is to introduce small asymmetries in the nanocluster oligomer, thus relaxing the orthogonal condition between the bright-electric and the dark-magnetic modes. In such a case, the Fano formation at the frequency of interest can be simply controlled and manipulated by carefully adjusting the nanostructure size and the inter-particle separations g (see Figure 3C, right panels). For values of g that are greater than 10 nm, only a weak interaction between the constituent dimers is established and a broad dipolar peak characterizes the metamolecule optical response, as it was retrieved in the

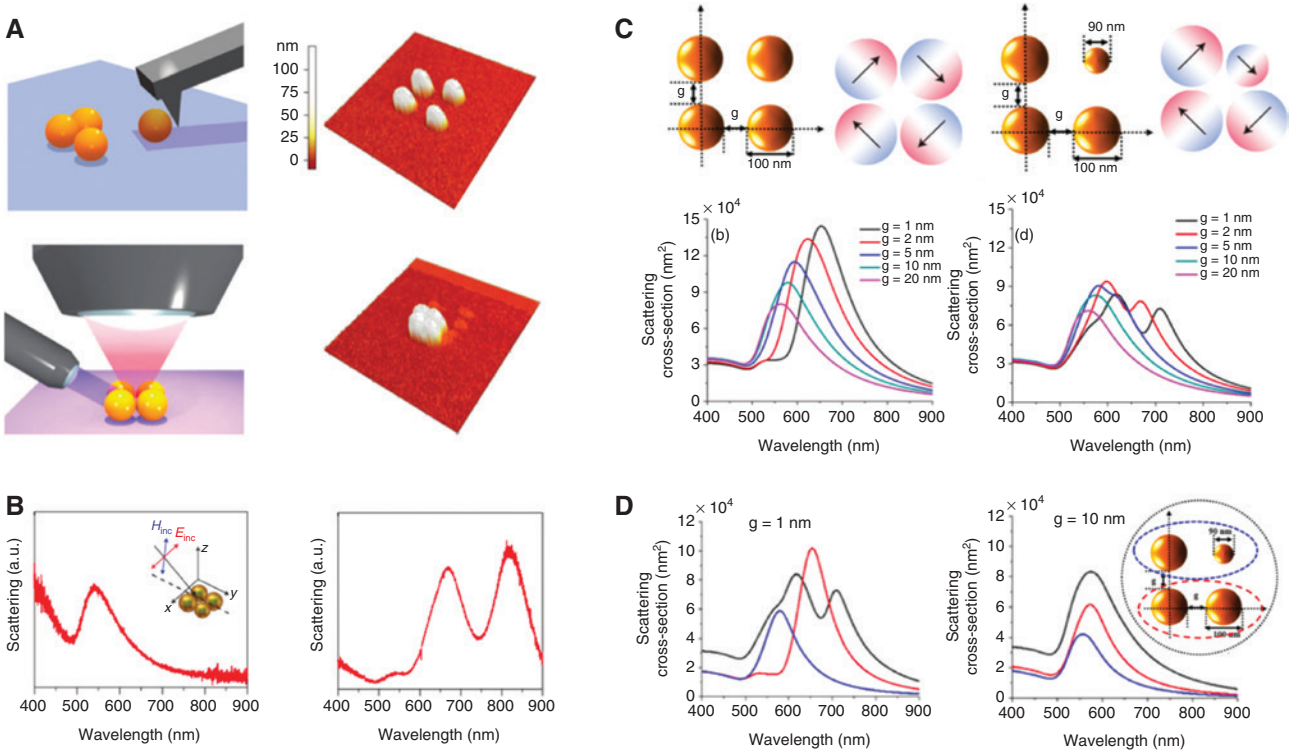

Figure 3: Plasmonic hybridization and Fano resonances.
(A) Left, schematic of the AFM manipulation and optical scattering setup. Right, AFM images of the gold oligomers over an area of 1.25 μm × 1.25 μm. (B) Measured scattering spectra when the four nanoparticles are far apart (left) and when they are arranged in a square aggregation with small gaps (right). The inset illustrates the experimental geometry and corresponding coordinate system. Reprinted by permission from from Springer Nature, Nat Nanotechnol 2013;8:95–9 A subwavelength plasmonic metamolecule exhibiting magnetic-based optical Fano resonance. Shafiei F, Monticone F, Le KQ, et al. (Ref. [51]) Copyright 2013 Springer Nature Limited. (C) Scattering cross-sections of the symmetric (left) and asymmetric (right) gold metamolecules for various interparticle distances *g*. In the symmetric case, the overall response of the system is dominated by the dipolar plasmon resonance of the single constituent, whereas the clustering of nanoparticles causes increased modes overlap and amplification of the scattering magnitude. In addition, the ring mode presents an overall net zero dipole moment and no Fano resonance is possible. Introducing a small asymmetry, for large interparticle distance the scattering cross section resembles the response of the isolated system, but for $g < 5$ nm, the signatures for strong coupling between nanodimers are observed in the onset of a Fano resonance. (D) The mechanism behind the Fano formation. The optical response of the isolated constituent of the asymmetric oligomer shown in the inset was studied. While the dipolar plasmon resonance of the top dimer (blue curves) shifts to the single sphere's LSPR, that of the bottom dimer (red curves) shifts to longer wavelengths. As the highest bright mode of the bottom dimer couples with the low dark mode of the top dimer, destructive interference between these modes results in a Fano dip in the scattering cross-section spectrum (black curves). Reprinted from Le KQ, Alù A, Bai J. Multiple Fano interferences in a plasmonic metamolecule consisting of asymmetric metallic nanodimers. J Appl Phys 2015;117:23118 (Ref. [93]), with the permission of AIP Publishing.

symmetric case. Conversely, for smaller inter-particle separations, the nanodimers plasmons strongly interact and interfere, giving rise to an asymmetric Fano-like dip in the scattering spectrum. Decoupling of the contributions of the upper and lower nanodimers allows for a better understanding of the physics behind the Fano formation. In fact, upon gap reduction, destructive interference is the result of the strong coupling between the highest bright mode of the bottom dimer and the low dark mode of the asymmetric one (see Figure 3D).

Following this idea, Nazir et al. [96] have realized a planar asymmetric disk trimer, which supports intense and localized magnetic hot-spots in the near infrared spectral range (see Figure 4A). A diameter increase of one of the three sub-units induces phase retardation effects between the resonance modes of the lower dimer and upper disk. When the interfering modes are spectrally overlapped, resonant hybridization occurs accompanied by a circulating displacement current with associated electric and magnetic hot-spots confined in the inter-particle regions. This coil mode corresponds to a sharp and pronounced Fano dip in the extinction spectrum, which is extremely sensitive to both the structural parameters and the surrounding refractive index. Within this context,

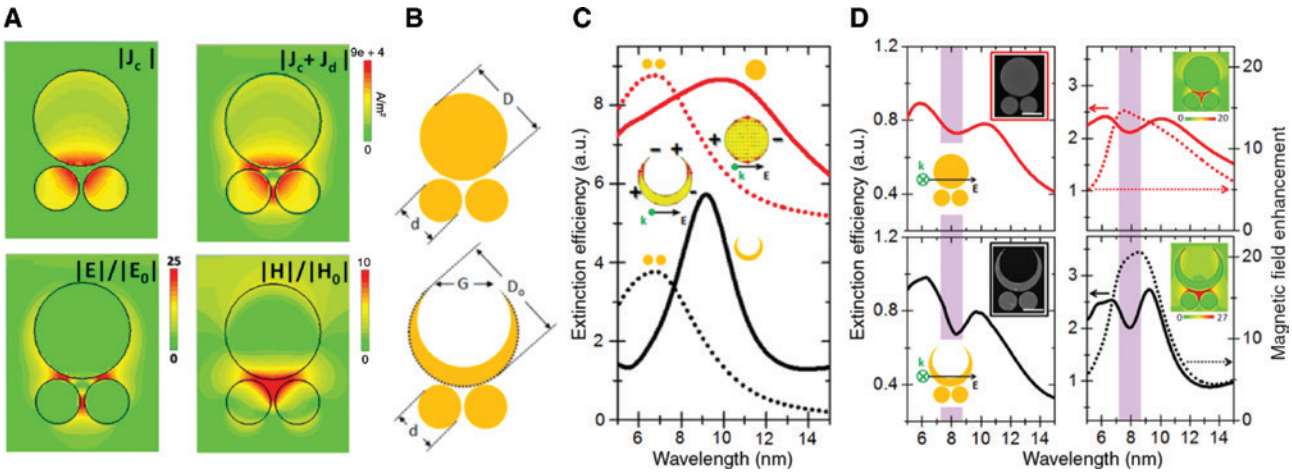

Figure 4: Coil-like dark modes and plasmonic hybridization involving high order modes.
(A) 2D plots of conduction current density (top left) and total charge current density, i.e. conduction plus displacement current (top right), together with the electric (bottom left) and magnetic field enhancement (bottom right) at the Fano resonance. Adapted with permission from Nazir A, Panaro S, Proietti Zaccaria R, Liberale C, De Angelis F, Toma A. Fano coil-type resonance for magnetic hot-spot generation. Nano Lett 2014;14:3166–71 (Ref. [96]). Copyright 2014 American Chemical Society. (B) Sketches depicting the main morphological parameters of the disk (upper sketch) and moon (lower sketch) trimers. (C) The respective simulated extinction efficiency spectra of the disk dimer (dotted curve) and single disk (continuous curve) in the disk trimer (upper red curves) and the extinction efficiency spectra of the disk dimer (dotted curve) and moon structure (continuous curve) in the moon-integrated trimer (lower black curves). (D) Left, experimental extinction efficiency spectra associated with the respective arrays of disk trimer (red curve) and MTR (black curve), for normal incidence condition (see the left side insets for the polarization direction). The insets respectively show the SEM images of a single disk trimer (upper inset) and a single MTR (lower inset) (scalebar: 1 μm). Right, respective simulated extinction efficiency spectra (solid lines) and magnetic field enhancement spectra (dotted lines) of the disk trimer array (red curves) and the MTR array (black curves). The insets show the 2D plots of the magnetic field enhancement distribution in the Fano resonance condition ($\lambda = 8$ μm). Adapted with permission from Panaro S, Nazir A, Proietti Zaccaria R, et al. Plasmonic moon: a Fano-like approach for squeezing the magnetic field in the infrared. Nano Lett 2015;15:6128–34 (Ref. [97]). Copyright 2015 American Chemical Society.

Panaro et al. have recently introduced another architecture supporting near-field hybridization between electric and magnetic resonances in the mid-infrared spectral range [97] (see Figure 4B). In this case, the superposition of a high-order plasmonic mode, which is supported by a crescent-like structure, and a dipolar resonance sustained by an underlying nanodisk dimer, promotes two different near field configurations: (i) an in-phase coupling that presents a non-vanishing electric dipole moment and (ii) an out-of-phase oscillation, with an almost-zero electric dipole moment but an intense magnetic response. In comparison to the spectral behavior of the asymmetric disk trimer (Figure 4C, red curve), the resonance of the crescent-like structure is more efficient in terms of sharpness and intensity (black curve, Figure 4C), positively affecting the localized and enhanced magnetic field supported by the system. In both cases, the magnetic field is perpendicularly oriented with respect to the oligomer plane and squeezed in the nanoscale region comprised between the disks and the upper element (see 2D plots of field distribution in Figure 4D). It is worth noting that the contributions in terms of field enhancement and confinement are greater for the crescent-like structure. As can be observed in Figure 4D (dotted lines), the magnetic field enhancement peaks are spectrally located in correspondence of the extinction peaks, thus confirming the magnetic resonant nature of the investigated modes. Moreover, the typical spectral features characterizing a Fano interference, such as extra-transparency and spectral sharpness, are further emphasized by the introduction of the crescent-like nanostructure.

Most of the architectures investigated thus far present optical magnetism only in a narrow spectral window and feature a net magnetic moment, associated to the pseudo-currents supported by electric plasmon resonances, orthogonal to the substrate. With the aim of broadening the spectral response of the magnetic resonance without increasing the resistive losses, 2D vertically stacked plasmonic assemblies have been introduced by Verre and coworkers [48]. The proposed architecture comprises a metal-insulator-metal (MIM) structure, which acts as an artificial meta-atom and promotes the efficient generation of a magnetic hot-spot, extremely concentrated in the tiny insulating layer (see the cartoon in Figure 5A). In

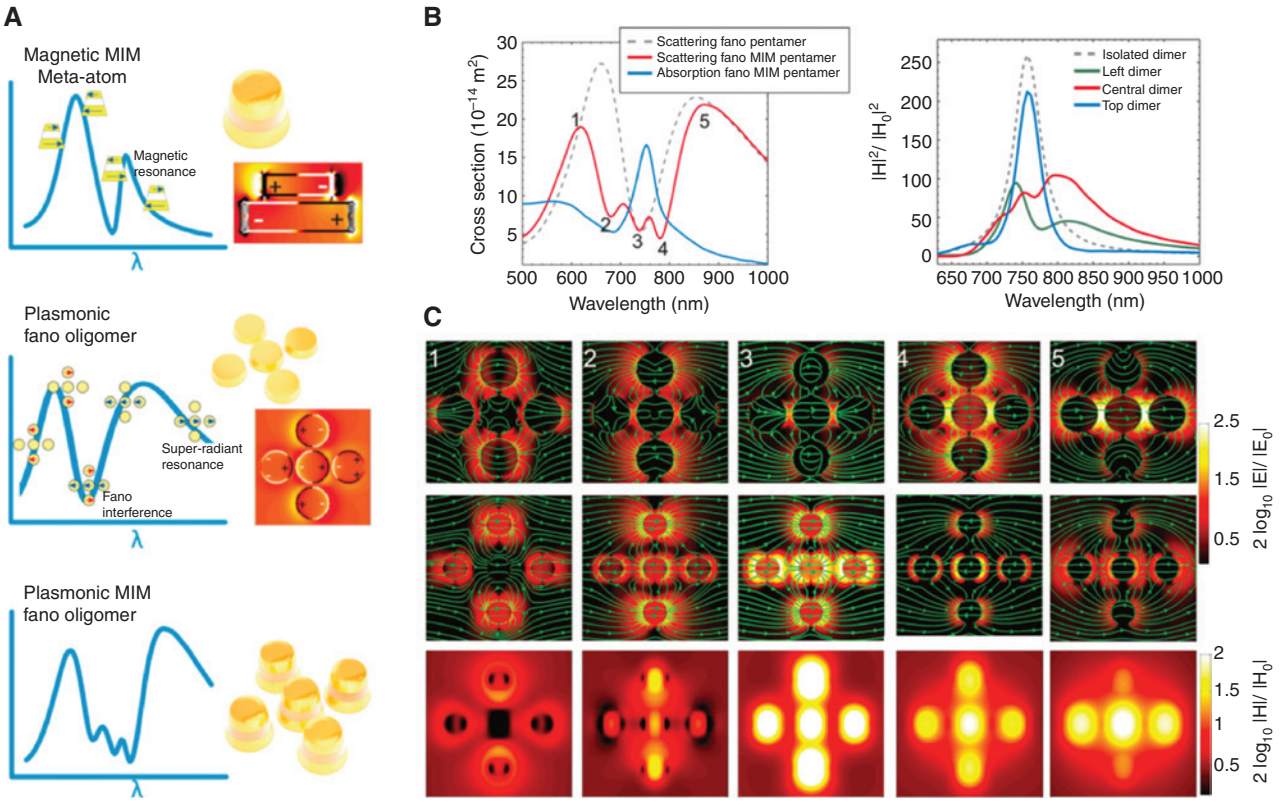

Figure 5: Magnetic resonance broadening in the optical regime.
(A) The scattering properties of a single vertical MIM dimer (top), plasmonic oligomer (centre) and MIM oligomer (bottom). The properties of the first two architectures are combined in the latter system that supports multiple subradiant modes, thus generating a quasi-broadband magnetic response at visible frequencies. (B) Left, simulated spectral response of a MIM pentamer (solid lines) and a standard gold pentamer (dashed line). Right, calculated magnetic field at the center of the dielectric spacer for the different vertical dimers in the MIM pentamer (solid lines). As a comparison, the magnetic enhancement for an isolated dimer is also shown (dashed line). (C) Electric field intensity and field lines at the center of the bottom disk (first row), top disk (second row) and magnetic field in the dielectric spacer at the wavelengths indicated by 1–5 in (B). Adapted with permission from Verre R, Yang ZJ, Shegai T, Käll M. Optical magnetism and plasmonic Fano resonances in metal–insulator–metal oligomers. Nano Lett 2015;15:1952–8 (Ref. [48]). Copyright 2015 American Chemical Society.

fact, for sub-10 nm thicknesses of the dielectric spacer, this oligomer exhibits a clear dip in the extinction spectrum, imputable to a magnetic resonance and identified by an antiphase oscillation of the electric dipoles in the metallic disks (Figure 5A, top panel). It follows that the resultant magnetic dipole lies in the plane of the magnetic meta-atom, aligned perpendicularly with respect to the electric dipoles and located in the insulating layer (see field distributions in Figure 5A). Following the same principles, when several magnetic meta-atoms are arranged in a pentamer configuration, multiple Fano resonances arise in the overall optical response, suggesting a non-trivial mutual interaction (see sketch and spectral response depicted in Figure 5A, bottom panel). This spectral behavior is significantly different from a metal oligomer, which features only a single Fano lineshape (see Figure 5A, middle panel). The present hybrid architecture displays a spectrally increased transparency window (as wide as ~150 nm) with an intricate fine-structure reflecting the complex couplings among the system constituents. The type and the number of hybridized resonances can be controlled with fine tuning of the interparticle distance and the dielectric thickness of each unit. The optical response of the magnetic meta-atom pentamer is displayed in Figure 5B for optimized parameters, together with the electric and magnetic near-field distributions for a few selected wavelenghts (highlighted in Figure 5C). The resonance at 613 nm (position 1 in Figure 5B, left panel) corresponds to the in-phase excitation of the MIM elements. At position 2, only the top metallic disks in each MIM are efficiently excited, but the three particles in the central row show a π-phase offset, resulting in a net vanishing dipole moment of the whole structure. All the features at longer wavelengths can be explained by the presence of a broad super-radiant continuum, generated by the bottom disks in the central row, superimposed

with multiple sharp dips attributed to various dark states and associated to the antiphase charged oscillations of the bottom and top metallic layers. The magnitude of the magnetic field enhancement within the spacer, illustrated in the bottom row of Figure 5C, is a clear indication of the virtual current loop and the corresponding magnetic dipole strength. Given that the incident field is polarized along the x-direction, i.e. aligned with the pentamer central row, different behaviors are found for the left, top and central MIM elements, as highlighted in Figure 5B (left panel). Despite its complex nature, the architecture presented here allows for a very broad magnetic response at visible frequencies, thus offering another intriguing perspective in the further manipulation of artificial magnetic response.

Owing to the inherent sharp spectral features and extreme field localization/enhancement associated with magnetic dark modes, plasmonic oligomers have enabled the realization of nanoscale platforms for surface-enhanced spectroscopies [67] and non-linear light generation [68].

Employing a practical bottom-up fabrication scheme, Chen and coworkers [67] have recently taken advantage of the so-called nanoparticle-on-mirror geometry [98, 99] for generating magnetic resonances at visible-near-infrared frequencies, thus facilitating the significant amplification of Raman signals. Very small nanogaps (in the order of 1 nm) are obtained in a highly reproducible manner by simply sandwiching a molecular monolayer between a gold nanosphere and an underlying single-crystal flat metallic surface, as it is schematically reproduced in Figure 6A. Upon light illumination and for small nanogaps, anti-symmetric charge distributions are excited at the nanoparticle surface and on the mirror imaging sphere (see the cartoon in Figure 6A right side). This phenomenon is well exemplified in the framework of plasmon hybridization between the modes supported by closely spaced nanoparticles [98]. This anti-parallel configuration is accompanied by a vanishing net dipole moment and, in analogy with other configurations, a circular displacement current that is typical of dipolar magnetic modes arises in the nanogap region. A near-field investigation of the system behaviour at the magnetic resonance frequency helps obtain further insights into the resonance mechanism. Interestingly, the 2D electric and magnetic near-field maps shown in Figure 6B demonstrate the co-localization of electric and magnetic hot-spots in the nanogap, a characteristic that plays a key role for applications in enhanced spectroscopies. Indeed, the co-existence (both spatially and in the frequency domain) of electric and magnetic resonances strongly enhance the SERS signal coming from the mercapto benzoic acid (MBA) molecules in the hot-spot region. This is shown in the Raman spectra of Figure 6C, acquired for different diameters of the gold nanosphere. The maximum signal is obtained when the magnetic dipolar mode perfectly matches the exciting laser line, thus indicating its crucial contribution to the overall sensitivity of the investigated platform.

The strongly confined and intense magnetic hot-spots supported by plasmonic oligomers help in dramatically boosting light-matter interactions in nanoscale volumes, with remarkable consequences for nonlinear optical processes as well. In this respect, adopting an

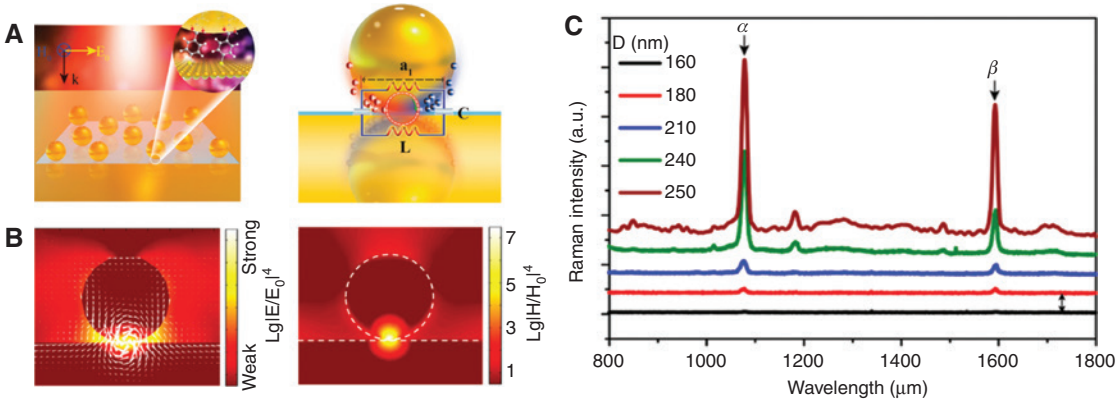

Figure 6: Magnetic resonance-enhanced Raman spectroscopy.
(A) Schematic illustration of the investigated coupled metallic nanosphere-film system and LC model at the magnetic dipolar mode. (B) The electric (left) and magnetic (right) field distributions at the magnetic resonance frequency. (C) The Raman signal of an MBA monolayer of molecules adsorbed on the flat gold film in the nanogap region, acquired for different values of the nanosphere diameter D. The labels α and β refer to the characteristic Raman lines of MBA. Adapted with permission from Chen S, Zhang Y, Shih TM, et al. Plasmon-induced magnetic resonance enhanced Raman spectroscopy. Nano Lett 2018;18:2209–16 (Ref. [67]). Copyright 2018 American Chemical Society.

asymmetric disk trimer similar to the one introduced by Nazir et al. [96] (see Figure 4B), Yang and coworkers [68] numerically investigated the magnetic resonance effects on the generation of second harmonic (SH) light. The destructive interference between the super-radiant electric mode of the upper disk with the sub-radiant magnetic mode of the nanoassembly gives rise to a sharp and pronounced transmission dip in the scattering spectrum (see black line in Figure 7A), accompanied by the formation of magnetic and electric hot-spots in the inter-particle regions (see inset in Figure 7A and B). Moreover, at the Fano resonance the radiative losses are efficiently suppressed and the absorption remains high (see red line in Figure 7A), thus producing no negative effect on the energy-harvesting capabilities of the oligomer and giving rise to a strong fundamental near-field located at its center. Consistent with this picture, the near field distribution map at the SH frequency for exctitation at the Fano dip shows high emission intensities, as highlighted in Figure 7C. Concurrently, the nanostructure far field calculated at the SH frequency exhibits the largest intensity when the fundamental excitation matches the dark magnetic resonance, thus unveiling the potentialities of magnetic modes for the efficient manipulation of nonlinear optical processes.

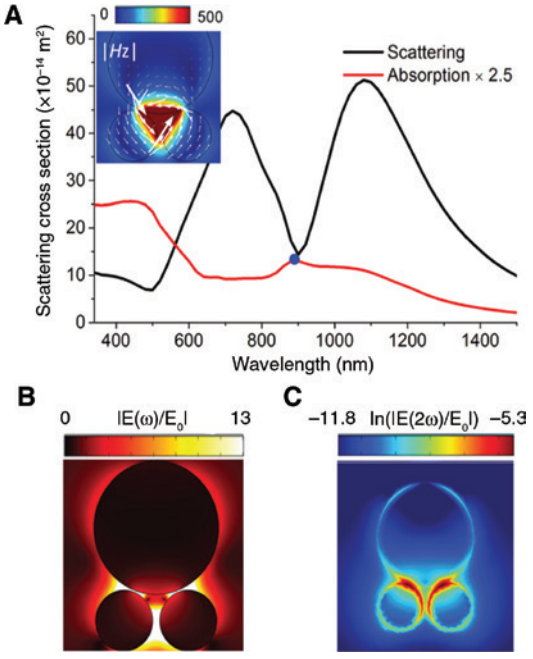

Figure 7: Magnetic Fano resonance-induced second harmonic generation.
(A) Scattering and absorption spectra of the oligomer in the vicinity of the magnetic Fano resonance. The inset shows the electric field distribution in the inter-particle region and the associated magnetic field excited at the magnetic dipole resonance. (B) Electric near-field enhancement map in the central plane of the trimer. (C) Near-field distribution of the electric field at the SH frequency for excitation at the magnetic Fano resonance. Adapted from Ref. [68] with permission from The Royal Society of Chemistry.

4 All dielectric nanoparticles

Nanostructured dielectric materials provide an alternative way to directly implement electric and magnetic field manipulation at visible/near infrared frequencies, thus suggesting a different approach to nano-photonics [52, 53]. Indeed, the observed EM-induced resonances can be capitalized for the efficient light concentration into deep-subwavelength volumes, in a selfsame way like noble metal plasmonic resonances. The simplest system, i.e. a single dielectric spherical nanoparticle, can exhibit both electric and strong magnetic resonances [100–102]. In fact, accordingly to Mie theory, the first fundamental mode of high-permittivity nanoparticles corresponds to a magnetic dipole excitation and originates from circular displacement currents driven by an incident electric field. The induced magnetic dipole moment lies in the plane that is perpendicular to the incident electric field and it is confined inside the dielectric nanoparticle. Even though these structures are endowed with lower near field enhancement compared with their conventional metallic counterparts, the induced magnetic dipole can be straightforwardly exploited as an additional degree of freedom in more complex all-dielectric assemblies. In analogy with a conventional metallic dimer, two coupled silicon nanoparticles support an electric field resonance and a corresponding hot-spot, for impinging radiation polarized along the interparticle main axis (see Figure 8A). In addition, for incident radiation polarized perpendicularly, a magnetic hot-spot arises in the nanogap region as a result of induced in-phase magnetic dipole moments in each nanoparticle. With the aim of understanding the nature of the different modes, a numerical study of the system has been recently performed by Bakker and coworkers [57], following a multipole decomposition approach. For light polarized along the main axis of the dimer (see Figure 8B, left panel), the scattering spectrum reveals a single peak due to the overlap between the electric and magnetic resonances, which are associated with the enhancement of both the electric and the magnetic fields. While the former is concentrated in the nanogap, the latter is mostly located inside the nanoparticles, thus making it poorly accessible for practical applications. Vice versa, for the orthogonal polarization (Figure 8B, right panel), the scattering spectrum is characterized by a pronounced dip in the total

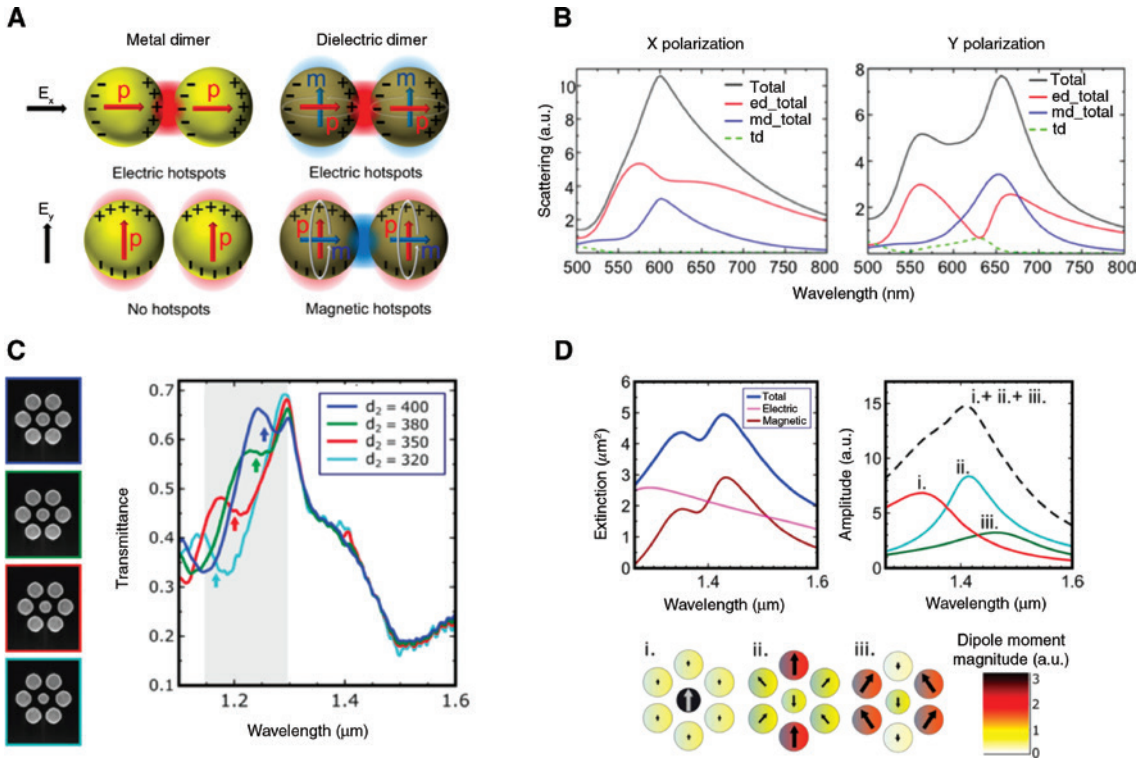

Figure 8: Recovering Fano-like magnetic modes through dielectric oligomers.
(A) Comparison of metallic (plasmonic) and dielectric nanodimers: dielectric nanoparticles support both electric and magnetic dipoles that couple with both orthogonal polarizations of the incident light field. (B) Numerical results for a silicon dimer. X- (left) and Y-polarized (right) light scattering spectra with mode decomposition. Adapted with permission from Bakker RM, Permyakov D, Yu YF, et al. Magnetic and electric hotspots with silicon nanodimers. Nano Lett 2015;15:2137–42 (Ref. [57]). Copyright 2015 American Chemical Society. (C) Left, scanning electron micrographs of the fabricated heptamer oligomers featuring different diameters of the central nanoparticle. Right, measured extinction spectrum of the oligomers. A Fano resonance is created in the heptamers (see gray-shaded region and colored arrows), and it moves across the spectrum as the diameter of the central particle d_2 is varied. (D) Top-left, simulated total extinction cross-section spectrum of the silicon disk heptamers (blue curve) and the electric (purple curve) and magnetic (red) contribution. Top-right, decomposition of the heptamer magnetic response into three eigenmodes (denoted as i–iii). Bottom, the distribution of the magnetic dipoles in each eigenmode. The Fano signature appear at intersection of eigenmodes i and ii. Adapted with permission from Chong KE, Hopkins B, Staude I, et al. Observation of Fano resonances in all-dielectric nanoparticle oligomers. Small 2014;10:1985–90 (Ref. [60]). Copyright 2014 Wiley-VCH Verlag GMBH & Co. KGaA, Weinheim.

electric dipole contribution, as a result of destructive interference between electric dipole and toroidal resonances [103], with the concurrent appearance of a magnetic hot-spot in the dielectric medium between the nanostructures. In this case, the toroidal dipole moment is generated by induced magnetic dipoles, which are not perfectly parallel due to the electric – magnetic dipole interaction. This feature is a unique property of the present system without a direct analogue in its metallic counterpart. For both X- and Y-polarized light the near-field behaviour displays a magnetic character, while higher hot-spot enhancement is obtained for Y-polarized light (over 6 times) in comparison to the X-polarized case (~3 times). This result establishes the former configuration as the most prominent case for spectroscopic applications.

The possibility of exciting both electric and magnetic resonances in the sub-units of all-dielectric oligomers has paved the way for their collective modes engineering. In particular, the concept of Fano resonance has been extended to dielectric systems by considering the mutual interference between their magnetic modes, thus offering an alternative route to achieve optical magnetism [58, 59]. In analogy with the metallic heptamer presented earlier, Chong and coworkers [60] realized a silicon counterpart, analyzing its spectral response both theoretically and experimentally. As shown in the extinction spectra of Figure 8C, two features are present for each considered configuration: the peak at longer wavelengths is stationary and associated to a magnetic resonance of the collective structure, whereas the one at shorter wavelengths

corresponds to the magnetic resonance of the central particle with an associated spectral shift depending on the particle diameter. The extra-transparency window between these two modes exhibits the typical asymmetric line-shape of Fano resonances characterized by resonant extinction suppression. Given the symmetry of the system, the contribution of the electric and magnetic resonances of the heptamer to the extinction cross-section can be completely separated and Fano interference is only observed for the magnetic contribution (see Figure 8D), which is given by the summation of three different eigenmodes (denoted here as resonances i–iii). The superposition between modes i and ii (see both spectra and sketches in Figure 8D) gives rise to the Fano resonance that is visible in the overall extinction spectrum: the former presents a magnetic dipole distribution that is heavily concentrated on the central nanodisk and thus very sensitive to its diameter. In comparison, the latter is characterized by a dipole distribution that is delocalized over the entire heptamer with a small fraction concentrated on the central nanodisk; thus, it is not significantly influenced by a size variation. The spectral position of the Fano resonance is located at the intersection of the resonance curves of the two modes and is strongly dependent on the geometrical parameters of the oligomer sub-units (i.e. arrangement, geometry and inter-particle separation).

Several approaches to fine-tune the Fano mechanism have been proposed so far. Within this framework, a comprehensive description of its origin has been provided through the near-field mapping of the Fano resonances in ceramic oligomers [104]. In particular, a heptamer of dielectric particles has been considered in the microwave region, where the far- and near-field responses have been assessed with high precision for both phase and intensity. Interestingly, a resonant suppression of the forward scattering has been observed in correspondence of the Fano interference between the magnetic resonance of the central particle and the collective response of the surrounding hexamer ring. The presence of the Fano resonance has been further confirmed by mapping the phase of the magnetic near-field across the heptamer structure.

On these bases, the study of magnetic Mie resonances in all-dielectric nanoparticles represents an alternative ingredient for light manipulation at the nanoscale. In particular, the ability to support both electric and magnetic modes within a single nanostructure is of great importance, being among the keystone principles of artificial metamaterials [105, 106]. The interplay between resonant modes can lead to strong effects on the particle scattering properties, including directional radiation effects [56], ad-hoc beam shaping [62], beam phase control for Huygens´ metasurfaces [107] and perfect absorption [108]. Indeed, in the case of overlapping electric and magnetic resonances, backward scattering can be limited and even suppressed, provided that the two interacting modes have the same strength. When this configuration is achieved, the relative extinction peaks of the interfering modes become significantly suppressed, resulting in a wavelength region of increased transparency (approaching the $T=1$ line) and enhanced resonant forward scattering [61]. Interestingly, the interaction between electric and magnetic modes can unleash alternative pathways in different nanophotonic domains, including, for example, optical trapping [72, 73, 109] and non-linear light generation [69, 110, 111].

In this respect, the optical binding forces exerted between pairs of resonant dielectric nanostructures can be efficiently tailored through several parameters, such as inter-particle distance, surrounding refractive index, polarization and wavelength of the excitation source [72], thus providing valuable tools for the realization of innovative platforms for optically controlled sorting and self-assembly of multiple high-index dielectric nanoparticles. As a matter of fact, properly designed silicon nanodimers exhibit attractive optical forces in air, but become repulsive in water at certain wavelengths [73], contrary to their metallic counterparts, which always display attractive forces over the entire visible region. The repulsion effect arises from the near-field interplay between the electric and magnetic modes, which uniquely occurs for dielectric nanoparticles, in the same spectral region. Decomposition into electric and magnetic dipole contributions helps reveal the underlying mechanism (see Figure 9A). Upon gradual refractive index (n) increase from air to water, the broad electric dipole resonance shifts to longer wavelengths and decreases in intensity. The magnetic contribution, instead, is characterized by two hybridized peaks (an induced electric contribution and a pure magnetic dipole), which feature an opposite trend for increasing values of n. As a consequence, the optical binding force (bottom of Figure 9A) between the nanoparticles immersed in an aqueous medium changes sign and becomes repulsive. The coupling strength can be controlled by adjusting the refractive index variation at the boundary between nanoparticles and dielectric medium: a decreasing of the refractive index contrast, indeed, induces a higher penetration of the EM field inside the surrounding medium together with an increased near-field interaction. An in-depth investigation of the near-field characteristics of the coupled system furnishes a clearer insight of the phenomenon (see Figure 9B). For all the considered wavelengths, the incident field is strongly localized in the inter-particle

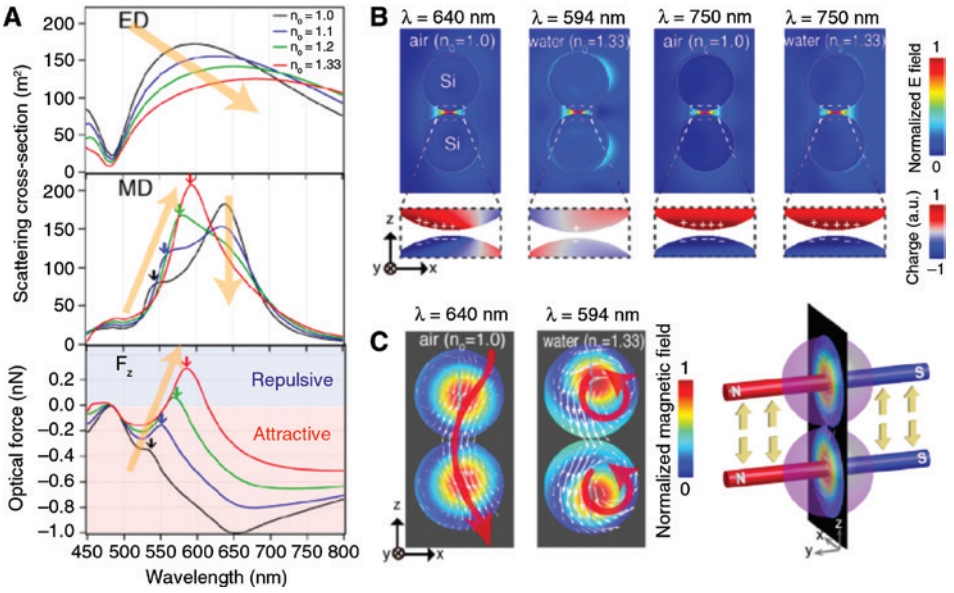

Figure 9: Magnetic optical binding forces.
(A) Scattering spectra of the electric dipole (ED) and magnetic dipole (MD) modes and optical binding force of the Si nanodimer calculated for surrounding refractive index (n_0) increase from 1.0 to 1.33. (B) Electric field distribution and surface charge density at different wavelengths in air and water. (C) Left, magnetic field distribution and current flow at 640 nm and 594 nm. Right, schematic representation of the repulsive force generated at 594 nm in water owing to the magnetic Lorentz force. Adapted with permission from Ref. [73], 2017 Optical Society of America.

separation (for both water and air media) with opposite charges facing each other and the resulting generation of an attractive force. However, the charge density for the magnetic dipole resonance in water (~594 nm) is much lower than the remaining cases, giving rise to a smaller attractive interaction. Concurrently, magnetic dipoles pointing in the same direction are generated by circularly flowing currents inside each dielectric nanoparticle (see Figure 9C), giving rise to a net repulsive force at the magnetic dipole resonant wavelength.

Furthermore, the ability of high-permittivity dielectric nanoparticles to simultaneously support electric and magnetic multipoles can be exploited to trigger optical nonlinearities in the nanostructured materials [112]. In particular, the III-V group semiconductors exhibit nonlinear phenomena that can benefit the enhancement provided by EM resonances. Typically, disk arrays are fabricated out of $Al_xGa_{1-x}As$ thin films [69, 112], whose direct band gap increases with Al concentration (x) and exhibit a strong quadratic optical nonlinearity that has been intrinsically linked to their crystalline structure. In this respect, Gili et al. [69] have recently realized monolithic $Al_xGa_{1-x}As$ nanocylinders on aluminum-oxide substrates, supporting a dipole resonance with a predominant magnetic character in the near-infrared spectral range, as can be seen in the electric field distribution map (Figure 10A, left panel) and in the multiple decomposition analysis (see Figure 10A, middle panel). Careful adjustment of the nanodisk structural parameters allows the coupling of its magnetic dipole resonance to the pump laser wavelength, thus boosting second harmonic generation (SHG) mechanisms. Employing a nonlinear microscopy setup, they were able to detect the SHG signal coming from individual nanopillars with conversion efficiency of high as 10^{-5}, while keeping other processes like third harmonic generation and multi-photon luminescence almost undetectable (see Figure 10A, right panel).

Similar results can be obtained considering the magnetic mode supported by a silicon nanodisk and the third-order term of the susceptibility tensor [70, 71]. In this configuration, an array of Si nanodisks was exploited by Shcherbakov and coworkers [70] to significantly enhance the third harmonic generation (THG) signal in proximity of their magnetic resonance. Decomposing the scattering cross-section of an individual silicon nanodisk into the electric and magnetic dipole contributions allows the identification of two distinct modes (see Figure 10B, left panel): a broad resonance at shorter wavelengths with an electric dipole character and a sharp magnetic dipole resonance at longer wavelengths. These findings are further confirmed by electric field maps reported in Figure 10B, middle panel, which exhibit a typical circulating current loop in the silicon nanodisk in correspondence of the magnetic resonance frequency. Importantly, the local field enhancement at the center of the nanodisk is a factor of 2 larger for the magnetic mode, making it the ideal candidate for

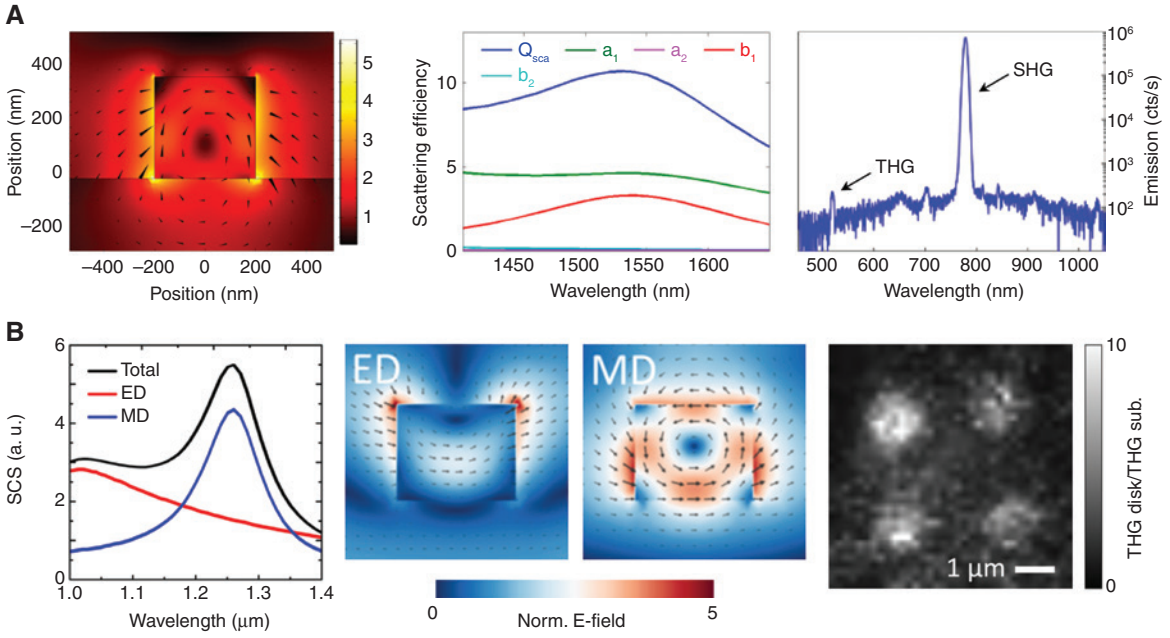

Figure 10: Non-linear light generation.
(A) From left to right, electric field enhancement map in the cross-sectional plane of a monolithic aluminum gallium arsenide (AlGaAs) nanoantenna and its scattering efficiency (Q_{sca}), with the multiple expansion terms. The coefficients a_1, b_1, a_2 and b_2 are due to the electric dipole, magnetic dipole, electric quadrupole and magnetic quadrupole contributions, respectively. SH emission spectrum of the optimized structure for the 500 μW incident power Adapted with permission from Ref. [69], 2016 Optical Society of America. (B) From left to right, numerical scattering cross-section spectra of the nanodisks (black curve) decomposed in the electric dipole (red curve) and magnetic dipole (blue curve) contributions with corresponding electric field distribution maps in the cross-sectional plane. Scanning optical microscope image detecting the THG signal coming from the nanostructures and normalized to the signal acquired from the substrate area. Adapted with permission from Shcherbakov MR, Neshev DN, Hopkins B, et al. Enhanced third-harmonic generation in silicon nanoparticles driven by magnetic response. Nano Lett 2014;14:6488–92 (Ref. [70]). Copyright 2014 American Chemical Society.

THG processes. Using a confocal microscope, the radiation (centered at 1240 nm to match the magnetic dipole resonance of the nanodisks) was delivered onto the sample in a focal area comprising four nanodisks at a time. Moreover, by tuning the spectrometer to the region of the third harmonic radiation (at 420 nm), it was possible to image the nanodisks array. Through careful engineering of the resonant modes' spectral position, a nonlinear emission with an efficiency of 10^{-7} and an enhancement of 2 orders of magnitude with respect to the unstructured bulk silicon slab was obtained. As the THG signal scales with the cube of the local fields, it was also possible to reach third harmonic light intensities that were bright enough to be seen by naked eye, thus paving the way towards the realization of breakthrough applications in nonlinear optics.

5 Conclusions

The field of artificial optical magnetism, boosted by the development of advanced fabrication techniques, has become an active research topic in the last years. On the one hand, the introduction of complex architectures and plasmonic oligomers inspired by the SRR geometry has allowed the shifting of the magnetic properties of metamaterials into the visible/near-infrared spectral range with outstanding results. Indeed, the exploitation of enhanced circulating displacement currents and extremely pronounced Fano resonance effects in plasmonic metamolecules has pushed further the nanoscale manipulation of optical magnetism at visible frequencies, thus suggesting alternative approaches to nanophotonic applications such as surface-enhanced spectroscopies, superlenses and non-linear light generation. On the other hand, the employment of high-index dielectric nanoparticles has facilitated the achievement of a remarkable magnetic response overcoming the inherent losses of plasmonic materials. The capability to sustain Mie resonances, both electric and magnetic in nature, has raised considerable interest towards the exploitation of dielectric nanoparticles for wavefront and polarization engineering as well as optical trapping and non-linear phenomena. Nevertheless, both counterparts represent ideal candidates

for the realization of novel platforms in many interdisciplinary areas of research, unveiling outstanding perspectives in the quest towards artificial optical magnetic materials.

Acknowledgments: A.C. and A.T. are grateful for the financial support from Compagnia di San Paolo under grant agreement ID ROL 10262. R.P.Z. acknowledges the support of the 3315 Innovative Teams Program of Ningbo-China (Grant No. Y70001DL01).

References

[1] Boltasseva A, Atwater HA. Low-loss plasmonic metamaterials. Science 2011;331:290–91.
[2] Baldassarre L, Sakat E, Frigerio J, et al. Midinfrared plasmon-enhanced spectroscopy with germanium antennas on silicon substrates. Nano Lett 2015;15:7225–31.
[3] Garoli D, Calandrini E, Bozzola A, et al. Fractal-Like plasmonic metamaterial with a tailorable plasma frequency in the near-infrared. ACS Photonics 2015;5:3408–14.
[4] Cortie MB, McDonagh AM. Synthesis and optical properties of hybrid and alloy plasmonic nanoparticles. Chem Rev 2011;111:3713–35.
[5] Zhang C, Kinsey N, Chen L, et al. High-performance doped silver films: overcoming fundamental material limits for nanophotonic applications. Adv Mater 2017;29:1605177.
[6] Abb M, Albella P, Aizpurua J, Muskens, OL. All-optical control of a single plasmonic nanoantenna-ITO hybrid. Nano Lett 2011;11:2457–63.
[7] Rycenga M, Cobley CM, Zeng J, et al. Controlling the synthesis and assembly of silver nanostructures for plasmonic applications. Chem Rev 2011;111:3669–712.
[8] Wiley BJ, Im SH, Li ZY, McLellan J, Siekkinen A, Xia Y. Maneuvering the surface plasmon resonance of silver nanostructures through shape-controlled synthesis. J Phys Chem B 2006;110:15666–75.
[9] Malerba M, Alabastri A, Miele E, et al. 3D Vertical nanostructures for enhanced infrared plasmonics. Sci Rep 2015;5:16436.
[10] Hutter E, Fendler JH. Exploitation of localized surface plasmon resonance. Adv Mater 2004;16:1685–706.
[11] Willets KA, Van Duyne RP. Localized surface plasmon resonance spectroscopy and sensing. Annu Rev Phys Chem 2007;58:267–97.
[12] Zhao Q, Zhou J, Zhang F, Lippens D. Mie resonance-based dielectric metamaterials. Mater Today 2009;12:60–9.
[13] Chirumamilla M, Chirumamilla A, Roberts AS, et al. Hot-spot engineering in 3D multi-branched nanostructures: ultrasensitive substrates for surface-enhanced Raman spectroscopy. Adv Opt Mater 2017;5:1600836.
[14] Cao Y, Zhang J, Yang Y, Huang Z, Long NV, Fu C. Engineering of SERS substrates based on noble metal nanomaterials for chemical and biomedical applications. Appl Spectrosc Rev 2015;50:499–525.
[15] Chirumamilla M, Chirumamilla A, Yang Y, et al. Large-area ultrabroadband absorber for solar thermophotovoltaics based on 3D titanium nitride nanopillars. Adv Opt Mater 2017;5:1700552.
[16] Zhang X, Chen YL, Liu R-S, Tsai DP. Plasmonic photocatalysis. Reports Prog Phys 2013;76:046401.
[17] Butet J, Brevet P-F, Martin OJF. Optical second harmonic generation in plasmonic nanostructures: from fundamental principles to advanced applications. ACS Nano 2015;9:10545–62.
[18] Monticone F, Alù A. The quest for optical magnetism: from split-ring resonators to plasmonic nanoparticles and nanoclusters. J Mater Chem C 2014;2:9059–72.
[19] Papadakis GT, Fleischman D, Davoyan A, Yeh P, Atwater HA. Optical magnetism in planar metamaterial heterostructures. Nat Commun 2018;9:296.
[20] Raza S, Bozhevolnyi SI, Wubs M, Mortensen NA. Nonlocal optical response in metallic nanostructures. J Phys Condens Matter 2015;27:183204.
[21] Smith DR, Pendry JB, Wiltshire MCK. Metamaterials and negative refractive index. Science 2004;305:788–92.
[22] Shelby RA, Smith DR, Schultz S. Experimental verification of a negative index of refraction. Science 2001;292:77–9.
[23] Veselago VG, Narimanov EE. The left hand of brightness: past, present and future of negative index materials. Nat Mater 2006;5:759–62.
[24] Liberal I, Engheta N. Near-zero refractive index photonics. Nat Photonics 2017;11:149–58.
[25] Moitra P, Yang Y, Anderson A, Kravchenko II, Briggs DP, Valentine J. Realization of an all-dielectric zero-index optical metamaterial. Nat Photonics 2013;7:791–5.
[26] Kruk SS, Wong ZJ, Pshenay-Severin E, et al. Magnetic hyperbolic optical metamaterials. Nat Commun 2016;7:11329.
[27] Poddubny A, Iorsh I, Belov P, Kivshar Y. Hyperbolic metamaterials. Nat Photonics 2013;7:948–57.
[28] Panaro S, Ciracì, C. Nonlocal plasmonic response and fano resonances at visible frequencies in sub-nanometer gap coupling regime. ACS Photonics 2016;3:2467–74.
[29] Ciracì C, Urzhumov Y, Smith DR. Effects of classical nonlocality on the optical response of three-dimensional plasmonic nanodimers. J Opt Soc Am B 2013;30:2731–6.
[30] Shalaev VM. Optical negative-index metamaterials. Nat Photonics 2007;1:41–8.
[31] Klein MW, Enkrich C, Wegener M, Linden S. Second-harmonic generation from magnetic metamaterials. Science 2006;313:502–4.
[32] O'Brien S, McPeake D, Ramakrishna SA, Pendry JB. Near-infrared photonic band gaps and nonlinear effects in negative magnetic metamaterials. Phys Rev B 2004;69:241101.
[33] Liu N, Fu L, Kaiser S, Schweizer H, Giessen H. Plasmonic building blocks for magnetic molecules in three-dimensional optical metamaterials. Adv Mater 2008;20:3859–65.
[34] Shalaev VM, Cai W, Chettiar UK, et al. Negative index of refraction in optical metamaterials. Opt Lett 2005;30:3356–8.
[35] Yu N, Capasso F. Flat optics with designer metasurfaces. Nat Mater 2014;13:139–50.
[36] Veselago VG. Electrodynamics of substances with simultaneously negative electrical and magnetic permeabilities. Sov Phys Uspekhi 1968;10:504–9.
[37] Pendry JB, Holden AJ, Robbins DJ, Stewart WJ. Magnetism from conductors and enhanced nonlinear phenomena. IEEE Trans Microw Theory Tech 1999;47:2075–84.
[38] Rockstuhl C, Lederer F, Etrich C, Zentgraf T, Kuhl J, Giessen H. On the reinterpretation of resonances in split-ring-resonators at normal incidence. Opt Express 2006;14:8827–36.

[39] Zhou J, Koschny T, Kafesaki M, Economou EN, Pendry JB, Soukoulis CM. Saturation of the magnetic response of split-ring resonators at optical frequencies. Phys Rev Lett 2005;95:223902.
[40] Kuznetsov AI, Miroshnichenko AE, Fu YH, et al. Split-ball resonator as a three-dimensional analogue of planar split-rings. Nat Commun 2014;5:3104.
[41] Leonhardt U. Optical conformal mapping. Science 2006;312:1777–80.
[42] Pendry JB. Negative refraction makes a perfect lens. Phys Rev Lett 2000;85:3966–9.
[43] Campione S, Guclu C, Ragan R, Capolino F. Enhanced magnetic and electric fields via Fano resonances in metasurfaces of circular clusters of plasmonic nanoparticles. ACS Photonics 2014;1:254–60.
[44] Montoni NP, Quillin SC, Cherqui C, Masiello DJ. Tunable spectral ordering of magnetic plasmon resonances in noble metal nanoclusters. ACS Photonics 2018;5:3272–81.
[45] Lassiter JB, Sobhani H, Fan JA, et al. Fano resonances in plasmonic nanoclusters: geometrical and chemical tunability. Nano Lett 2010;10:3184–9.
[46] Mirin NA, Bao K, Nordlander P. Fano resonances in plasmonic nanoparticle aggregates. J Phys Chem A 2009;113:4028–34.
[47] Hentschel M, Saliba M, Vogelgesang R, Giessen H, Alivisatos AP, Liu N. Transition from isolated to collective modes in plasmonic oligomers. Nano Lett 2010;10:2721–6.
[48] Verre R, Yang ZJ, Shegai T, Käll M. Optical magnetism and plasmonic Fano resonances in metal–insulator–metal oligomers. Nano Lett 2015;15:1952–8.
[49] Lorente-Crespo M, Wang L, Ortuño R, García-Meca C, Ekinci Y, Martínez A. Magnetic hot spots in closely spaced thick gold nanorings. Nano Lett 2013;13:2654–61.
[50] Campione S, Liu S, BasilioLI, et al. Broken symmetry dielectric resonators for high quality factor Fano metasurfaces. ACS Photonics 2016;3:2362–7.
[51] Shafiei F, Monticone F, Le KQ, et al. A subwavelength plasmonic metamolecule exhibiting magnetic-based optical Fano resonance. Nat Nanotechnol 2013;8:95–9.
[52] Staude I, Schilling J. Metamaterial-inspired silicon nanophotonics. Nat Photonics 2017;11:274–84.
[53] Jahani S, Jacob Z. All-dielectric metamaterials. Nat Nanotechnol 2016;11:23–36.
[54] Kuznetsov AI, Miroshnichenko AE, Fu YH, Zhang J, Luk'yanchuk B. Magnetic light. Sci Rep 2012;2:492.
[55] Evlyukhin AB, Reinhardt C, Seidel A, Luk'yanchuk BS, Chichkov BN. Optical response features of Si-nanoparticle arrays. Phys Rev B 2010;82:45404.
[56] Staude I, Miroshnichenko AE, Decker M, et al. Tailoring directional scattering through magnetic and electric resonances in subwavelength silicon nanodisks. ACS Nano 2013;7:7824–32.
[57] Bakker RM, Permyakov D, Yu YF, et al. Magnetic and electric hotspots with silicon nanodimers. Nano Lett 2015;15:2137–42.
[58] Hopkins B, Filonov DS, Miroshnichenko AE, Monticone F, Alù A, Kivshar YS. Interplay of magnetic responses in all-dielectric oligomers to realize magnetic Fano resonances. ACS Photonics 2015;2:724–9.
[59] Miroshnichenko AE, Kivshar YS. Fano resonances in all-dielectric oligomers. Nano Lett 2012;12:6459–63.
[60] Chong KE, Hopkins B, Staude I, et al. Observation of Fano resonances in all-dielectric nanoparticle oligomers. Small 2014;10:1985–90.
[61] Liu W, Miroshnichenko AE, Neshev DN, Kivshar YS. Broadband unidirectional scattering by magneto-electric core–shell nanoparticles. ACS Nano 2012;6:5489–97.
[62] Gomez-Medina R, Garcia-Camara B, Suarez-Lacalle I, et al. Electric and magnetic dipolar response of germanium nanospheres: interference effects, scattering anisotropy, and optical forces. J Nanophotonics 2011;5:53510–2.
[63] Chen WT, Zhu AY, Sanjeev V, et al. A broadband achromatic metalens for focusing and imaging in the visible. Nat Nanotechnol 2018;13:220–6.
[64] Shcherbakov MR, Vabishchevich PP, Shorokhov AS, et al. Ultrafast all-optical switching with magnetic resonances in nonlinear dielectric nanostructures. Nano Lett 2015;15:6985–90.
[65] Makarov S, Kudryashov S, Mukhin I, et al. Tuning of magnetic optical response in a dielectric nanoparticle by ultrafast photoexcitation of dense electron–hole plasma. Nano Lett 2015;15:6187–92.
[66] Liu S, Sinclair MB, Mahony TS, et al. Optical magnetic mirrors without metals. Optica 2014;1:250–6.
[67] Chen S, Zhang Y, Shih TM, et al. Plasmon-induced magnetic resonance enhanced Raman spectroscopy. Nano Lett 2018;18:2209–16.
[68] Yang D-J, Im S-J, Pan G-M, et al. Magnetic Fano resonance-induced second-harmonic generation enhancement in plasmonic metamolecule rings. Nanoscale 2017;9:6068–75.
[69] Gili VF, Carletti L, Locatelli A, et al. Monolithic AlGaAs second-harmonic nanoantennas. Opt Express 2016;24:15965–71.
[70] Shcherbakov MR, Neshev DN, Hopkins B, et al. Enhanced third-harmonic generation in silicon nanoparticles driven by magnetic response. Nano Lett 2014;14:6488–92.
[71] Shorokhov AS, Melik-Gaykazyan EV, Smirnova DA, et al. Multifold enhancement of third-harmonic generation in dielectric nanoparticles driven by magnetic Fano resonances. Nano Lett 2016;16:4857–61.
[72] Lamothe É, Lévêque G, Martin OJF. Optical forces in coupled plasmonic nanosystems: Near field and far field interaction regimes. Opt Express 2007;15:9631–44.
[73] Yano T, Tsuchimoto Y, Zaccaria RP, Toma A, Portela A, Hara M. Enhanced optical magnetism for reversed optical binding forces between silicon nanoparticles in the visible region. Opt Express 2017;25:431–9.
[74] Linden S, Enkrich C, Wegener M, Zhou J, Koschny T, Soukoulis CM. Magnetic response of metamaterials at 100 terahertz. Science 2004;306:1351–3.
[75] Aydin K, Bulu I, Guven K, Kafesaki M, Soukoulis CM, Ozbay E. Investigation of magnetic resonances for different split-ring resonator parameters and designs. New J Phys 2005;7:168.
[76] Rockstuhl C, Zentgraf T, Guo H, et al. Resonances of split-ring resonator metamaterials in the near infrared. Appl Phys B 2006;84:219–27.
[77] Katsarakis N, Konstantinidis G, Kostopoulos A, et al. Magnetic response of split-ring resonators in the far-infrared frequency regime. Opt Lett 2005;30:1348–50.
[78] Soukoulis CM, Linden S, Wegener M. Negative refractive index at optical wavelengths. Science 2007;315:47–9.
[79] Corrigan TD, Kolb PW, Sushkov AB, Drew HD, Schmadel DC, Phaneuf RJ. Optical plasmonic resonances in split-ring resonator structures: an improved LC model. Opt Express 2008;16:19850–64.

[80] Rius G, Baldi A, Ziaie B, Atashbar MZ. In: Bhushan B, ed. Introduction to Micro-/Nanofabrication. Berlin, Heidelberg, Springer, 2017, 51–86.
[81] Chen WT, Chen CJ, Wu PC, et al. Optical magnetic response in three-dimensional metamaterial of upright plasmonic meta-molecules. Opt Express 2011;19:12837–42.
[82] Staude I, Decker M, Ventura MJ, et al. Hybrid high-resolution three-dimensional nanofabrication for metamaterials and nanoplasmonics. Adv Mater 2012;25:1260–4.
[83] Seet KK, Mizeikis V, Matsuo S, Juodkazis S, Misawa H. Three-dimensional spiral-architecture photonic crystals obtained by direct laser writing. Adv Mater 2005;17:541–5.
[84] Makarov SV, Zalogina AS, Tajik M, et al. Light-induced tuning and reconfiguration of nanophotonic structures. Laser Photon Rev 2017;11:1700108.
[85] Zilio P, Malerba M, Toma A, Zaccaria RP, Jacassi A, De Angelis F. Hybridization in three dimensions: a novel route toward plasmonic metamolecules. Nano Lett 2015;15: 5200–7.
[86] Li Y, Huo Y, Zhang Y, Zhang Z. Generation and manipulation of multiple magnetic Fano resonances in split ring-perfect ring nanostructure. Plasmonics 2017;12:1613–9.
[87] Dolling G, Enkrich C, Wegener M, Zhou JF, Soukoulis CM, Linden S. Cut-wire pairs and plate pairs as magnetic atoms for optical metamaterials. Opt Lett 2005;30:3198–200.
[88] Garcia-Meca C, Hurtado J, Martí J, Martínez A, Dickson W, Zayats AV. Low-loss multilayered metamaterial exhibiting a negative index of refraction at visible wavelengths. Phys Rev Lett 2011;106:67402.
[89] Liu N, Mukherjee S, Bao K, et al. Magnetic plasmon formation and propagation in artificial aromatic molecules. Nano Lett 2012;12:364–69.
[90] Luk'yanchuk B, Zheludev NI, Maier SA, et al. The Fano resonance in plasmonic nanostructures and metamaterials. Nat Mater 2010;9:707–15.
[91] Hopkins B, Poddubny AN, Miroshnichenko AE, Kivshar YS. Revisiting the physics of Fano resonances for nanoparticle oligomers. Phys Rev A 2013;88:53819.
[92] Alù, A., Salandrino A, Engheta N. Negative effective permeability and left-handed materials at optical frequencies. Opt Express 2006;14:1557–67.
[93] Le KQ, Alù A, Bai J. Multiple Fano interferences in a plasmonic metamolecule consisting of asymmetric metallic nanodimers. J Appl Phys 2015;117:23118.
[94] Fan JA, Bao K, Wu C, et al. Fano-like interference in self-assembled plasmonic quadrumer clusters. Nano Lett 2010;10:4680–5.
[95] Roller E-M, Khorashad LK, Fedoruk M, Schreiber R, Govorov AO, Liedl T. DNA-assembled nanoparticle rings exhibit electric and magnetic resonances at visible frequencies. Nano Lett 2015;15:1368–73.
[96] Nazir A, Panaro S, Proietti Zaccaria R, Liberale C, De Angelis F, Toma A. Fano coil-type resonance for magnetic hot-spot generation. Nano Lett 2014;14:3166–71.
[97] Panaro S, Nazir A, Proietti Zaccaria R, et al. Plasmonic moon: a Fano-like approach for squeezing the magnetic field in the infrared. Nano Lett 2015;15:6128–34.
[98] Liu N, Guo H, Fu L, Kaiser S, Schweizer H, Giessen H. Plasmon hybridization in stacked cut-wire metamaterials. Adv Mater 2007;19:3628–32.
[99] Chikkaraddy R, de Nijs B, Benz F, et al. Single-molecule strong coupling at room temperature in plasmonic nanocavities. Nature 2016;535:127–30.
[100] García-Etxarri A, Gómez-Medina R, Froufe-Pérez LS, et al. Strong magnetic response of submicron silicon particles in the infrared. Opt Express 2011;19:4815–26.
[101] Evlyukhin AB, Novikov SM, Zywietz U, et al. Demonstration of magnetic dipole resonances of dielectric nanospheres in the visible region. Nano Lett 2012;12:3749–55.
[102] Krasnok AE, Miroshnichenko AE, Belov PA, Kivshar YS. All-dielectric optical nanoantennas. Opt Express 2012;20: 20599–604.
[103] Kaelberer T, Fedotov VA, Papasimakis N, Tsai DP, Zheludev NI. Toroidal dipolar response in a metamaterial. Science 2010;330:1510–2.
[104] Filonov DS, Slobozhanyuk AP, Krasnok AE, et al. Near-field mapping of Fano resonances in all-dielectric oligomers. Appl Phys Lett 2014;104:21104.
[105] Lepetit T, Akmansoy É, Ganne J-P. Experimental measurement of negative index in an all-dielectric metamaterial. Appl Phys Lett 2009;95:121101.
[106] Xiao S, Drachev VP, Kildishev AV, et al. Loss-free and active optical negative-index metamaterials. Nature 2010;466:735–8.
[107] Cheng J, Ansari-Oghol-Beig D, Mosallaei H. Wave manipulation with designer dielectric metasurfaces. Opt Lett 2014;39:6285–8.
[108] Liu X, Zhao Q, Lan C, Zhou J. Isotropic Mie resonance-based metamaterial perfect absorber. Appl Phys Lett 2013;103:31910.
[109] Zhao R, Tassin P, Koschny T, Soukoulis CM. Optical forces in nanowire pairs and metamaterials. Opt Express 2010;18:25665–76.
[110] Carletti L, Locatelli A, Stepanenko O, Leo G, De Angelis C. Enhanced second-harmonic generation from magnetic resonance in AlGaAs nanoantennas. Opt Express 2015;23: 26544–50.
[111] Smirnova D, Smirnov AI, Kivshar YS. Multipolar second-harmonic generation by Mie-resonant dielectric nanoparticles. Phys Rev A 2018;97:13807.
[112] Kruk SS, Camacho-Morales R, Xu L, et al. Nonlinear optical magnetism revealed by second-harmonic generation in nanoantennas. Nano Lett 2017;17:3914–8.